Probing optoelectronic and thermoelectric properties of double perovskite halides Li_2CuInY_6 (Y = Cl, Br, I) for energy conversion applications

N. Ahmad Noor[a,*], F. Nasrullah[a], H. O. Elansary[b], S. Mumtaz[c]
[a]*Department of Physics, University of Lahore, Lahore 54000, Pakistan*
[b]*Plant Production Department, College of Food and Agriculture Sciences, King Saud University, P.O. Box 2460, Riyadh 11451, Saudi Arabia*
[c]*Electrical and Biological Physics, Kwangwoon University, Seoul, 01897, South Korea*

Recently, double perovskite halides (DPHs) become crucial due to their potential applications in optoelectronic devices due to their stability, non-toxicity, superior oxidation resistance, high conversion efficiency, and high temperature stability. In the current study, we explored DPHs Li_2CuInY_6 (Y = Cl, Br, I) employing Wien2k package to analyze the structural stability, optoelectronic and thermoelectric features. The formation energy and Born stability criteria are computed to confirm thermodynamic and structural stability. Studied DPHs have direct bandgaps nature investigated by modified Becke and Johnson (mBJ) potential. Calculated values of bandgap decreases, when replace halide ion from Cl to I, indicate tuning from visible to infrared (IR) region of electromagnetic spectrum. Their band edge tuning across the visible to infrared border is reliant on replacement, which makes them suitable for projects involving opto-electronic devices. Further, optical features are investigated in terms of incident photon energy in order to assess the optical output. Lastly, electronic thermoelectric performance is computed using the figure of merit (ZT) for all DPs. Computed results of direct bandgap and optical behavior show that DP $Li_2CuInCl_6$ can be used as photovoltaic devices as compared to DPs $Li_2CuInBr_6$ and Li_2CuInI_6.

(Received February 6, 2024; Accepted May 21, 2024)

Keywords: Halide double perovskites, Elastic constant, Direct bandgap, Absorption coefficient, Figure of merit

1. Introduction

Researchers have proposed a number of alternatives to the creation of power systems in order to lessen the dependence of people on conventional fossil fuel power generating processes [1]. This is because the pace of power depletion has been steadily increasing during recent centuries. The scientific community was inspired to invent and create innovative systems to convert heat into electrical energy since two-thirds of the created energy is wasted as heat. We are grateful for materials that can convert heat into power. The advantages of thermoelectric materials are their lack of noise, toxicity, lack of leakage residues, durability, and affordability. Thermoelectric energy conversion has emerged as an upcoming technique to convert extra heat from car and other production processes into usable energy [2-4]. Applications that use thermoelectric technology are reliable, safe for the environment, quiet, and devoid of moving components. This technology so represents an upcoming source of sustainable and clean energy. For thermoelectric applications, it has been observed that semiconductors with wide bandgaps and greater S and maximum power factor values make a trustworthy choice. A variety of innovative systems of materials were created in former times using the phonon glass and electron crystal models, which revealed high values for the ZT [5, 6].

Nevertheless, these thermoelectric materials can't be used at temperatures beyond 700 K since their constituent parts quickly melt and dissolve. Due to its lower price and increased

* Corresponding author: naveed.noor@riphah.edu.pk
https://doi.org/10.15251/JOR.2024.203.333

chemical and thermal stability, coated cobaltite with a favorable ZT value (0.3 at 1000 K) is therefore considered a viable option [7, 8]. Due to their enticing properties in a variety of applications, such as thermoelectricity, optoelectronics, and energy storage devices, researchers have been devoted to the formulation for double perovskite halides [9, 10]. Owing of their compositional instabilities, excessive moisture content, and environmental pollution, DPHs continue to be unsuitable for solar cell devices [11]. Lead was replaced with Bi and Ag in lead-based double perovskites due to these limitations, particularly lead's poisonous nature. Although their properties offer more compositional diversity and better control over the adjustment of many physical characteristics, Pb-free DPHs are now in demand [12].

Among DPHs, recently Li-based DPHs Li_2CuBiZ_6 (Z=Cl, Br and I) and Li_2AgGaX_6 (X = Cl, Br, I) explored theoretically for the manufacturing of optoelectronic and thermoelectric device applications using density functional theory [13, 14]. Their finding of direct bangap nature indicate all DPHs potential candidate for photovoltaic devices. In this study, we examine the potential of non-toxic double perovskites, especially the Li-based DPHs Li_2CuInY_6 (Y= Cl, Br, I) to achieve the efficiencies comparable to those of double perovskites based on lead. For instance, the utilization of Cu in place of B^+ and In in lieu of B^{3+} cations has appeared as a suitable strategy for designing nontoxic double perovskite halides [15]. We anticipate that the findings of our work will inspire future theoretical and practical research aimed at creating DPHs Li_2CuInY_6 in optoelectronic and power generation devices.

2. Computational details

We applied the FPLAPW+lo technique [16], which is based on density function theory (DFT), to examine the physical features of DPHs Li_2CuInY_6. A generalized gradient (PBEsol-GGA) approximation was used to look at structural characteristics. Additionally, the Tran-Blaha enhanced Becke-Johnson function was used to optimize the convergence energy and electrical structure, producing more accurate energy gap measurements [17, 18]. The electrical system's solution is reflected spherically harmonized in the muffin tin sphere but behaves as a plane wave in the interstitial region. Utilizing l = 10, Gmax = 16, the Gaussian parameter, the muffin radius and wave vector product in the reciprocal lattice, and $K_{max} \times R_{MT} = 8$, the basic characteristics are enhanced. 2000 k-points are used to choose the k-mesh in a 12 ×12 × 12 order so that the system's energy output is continuous. The precision of calculated results is limited by convergence threshold requirements [19]. The BoltzTraP algorithm, which is based on Boltzmann theory, was used to calculate the transport characteristics [20, 21].

3. Results and discussion

3.1. Structural stability and elastic features

As displayed in Fig. 1, the unit cell of the DPHs Li_2CuInY_6 indicate a cubic structure with the Fm-3m space group. The unit cell in polyhedral format is given in which green, blue, purple, and red balls, correspondingly stand in for the Li, Cu, In, and halogen (Cl/Br/I) atoms.

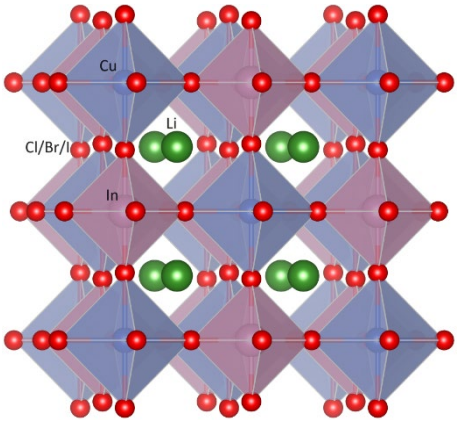

Fig. 1. Unit cell plot of DPs Li_2CuInX_6 (X = Cl, Br, I) halides in polyhedral format.

Lattice parameters are estimated using the PBEsol-GGA from volume optimization. Fig. 2 shows the calculated crystalline energy for all DPHs versus the volume plot. To get the ideal measurement for the lattice parameters at ground state, these graphs have been adjusted with the Birch Murnaghan equation of state [22]. According to Table 1, the calculated values of the lattice constant (a_0) are 10.36 for $Li_2CuInCl_6$, 10.95 for $Li_2CuInBr_6$, and 11.81 for Li_2CuInI_6. Evidently, the increase in atomic radius of Cl to I atoms involved causes the lattice constant increases. As shown in Table 1, the increase in cation size leads to an increase in interatomic pressure, which leads to a decrease in bulk modulus (B_0) value [23].

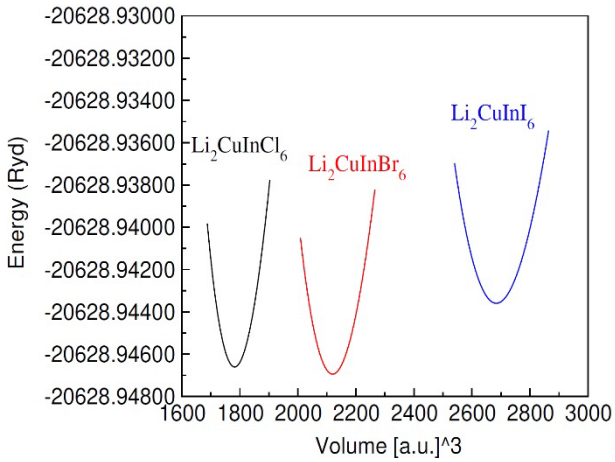

Fig. 2. Optimization plot of investigated double perovskites Li_2CuInX_6 (X = Cl, Br, I) halides.

To investigate thermodynamically stability for DPs Li_2CuInX_6 (X = Cl, Br, I), formation energy is calculated through the following connection:

$$\Delta H_f = E_{Total}(Li_aCu_bIn_cY_d) - aE_{Li} - bE_{Cu} - cE_{In} - dE_Y \quad (1)$$

The total energy of the compounds is shown above as E_{Total} ($Li_aCu_bIn_cY_d$), where E_{Li} stands for the energy of Li, E_{Cu} for that of Cu, E_{In} for that of In, and E_Y for Cl/Br/I atoms. The coefficients of E_{Li}, E_{Cu}, E_{In}, and E_Y are a, b, c, and d, respectively, and they display the number of atoms for each component of the formula unit [24]. The feasibility of every chemical reaction is

determined by the sign of ΔH_f. The absence of a positive indication signifies thermodynamic feasibility of the created product.

The mechanical parameters of DPHs Li_2CuInY_6 obtained from the tensor matrix [25] are shown in Table 1. To describe the mechanical properties of cubic systems, one just has to know the three elastic constants C_{11}, C_{12}, and C_{44}. These constants are connected to one another for stable cubic systems as $(C_{11}-C_{12})>0$, $C_{11}>0$, $C_{44}>0$ and $C_{12}>0$. The bulk modulus decreases as the lattice constant value increases, suggesting that the materials under research are less able to withstand applied stress as the atomic radius of halogen increases [26]. Prior to utilization of a deterministic approach to determine if a substance is brittle or ductile, an apparatus must be designed. By computing the Pugh's (B/G) as well as Poisson's (υ) ratios, it was eliminated. Such proportions have essential measurements for ductile materials, with B/G > 1.75 and υ> 0.26 [27, 28]. Table 1 shows that these compounds are flexible based on calculated values for both ratios. Pugh's ratio (B/G) measurements show that Li_2CuInI_6 is less ductile than the other two structures, with a measured ratio of 1.77 for $Li_2CuInCl_6$.

Table 1. Investigated values of a_o(Å): lattice constant, B_o(GPa): bulk modulus, ΔH_f: formation energy and elastic parameters of DPHs Li_2CuInX_6.

Parameters	$Li_2CuInCl_6$	$Li_2CuInBr_6$	Li_2CuInI_6
	PBEsol-GGA	PBEsol-GGA	PBEsol-GGA
a_o(Å)	10.18	10.79	11.67
B_o (*GPa*)	35.89	29.28	22.25
ΔH_f (eV)	-2.43	-2.19	-2.05
C_{11}	76.10	49.07	36.18
C_{12}	20.39	20.02	15.20
C_{44}	13.57	10.59	14.03
B	35.96	29.70	22.19
G	16.89	12.01	12.48
Y	43.86	31.75	31.54
B/G	2.13	2.47	1.77
υ	0.29	0.32	0.26

3.2. Optoelectronic features

Investigating the energy band dispersion is necessary to maximize a material's capacity to absorb incident electromagnetic radiations and may offer helpful information about the suitability of a material for the manufacture of sophisticated devices [31]. We explored the phenomena of structure relaxation in order to calculate the electronic band structure (BS), and we used mBJ potential to do so. The electronic band structures of all DPHs are shown in Fig. 3. Each composition exhibits the same trend in band structure, and the band edges' presence at the same symmetry point (Γ) indicates that they are suitable for optoelectronic applications due to their superior performance and direct energy gap nature [32]. The exact energy measurement utilizing the mBJ potential showed bandgap values of 1.34 eV for $Li_2CuInCl_6$, 0.84 eV for $Li_2CuInBr_6$, and 0.34 eV for Li_2CuInI_6. While the compositions with Br and I at the halogen site have the lowest bandgap value and might be employed in IR detectors, those with Cl as the base have bandgaps that are in the visible energy range, making them for photovoltaic devices. The bonding and hybridization with the compounds are influenced by the differing atomic sizes of Cl, Br, and I. Changes in atomic size have an impact on how closely atomic orbitals overlap and how much different atoms are hybridized, which changes the energy gap.

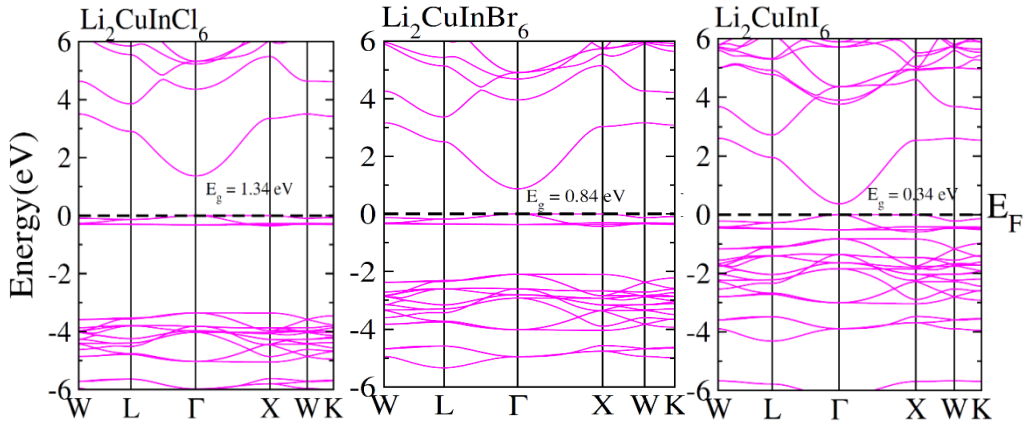

Fig. 3. Band structure plot for DPHs $Li_2CuInCl_6$, $Li_2CuInBr_6$ and Li_2CuInI_6.

Fig. 4 shows density of states (DOS) graphs for each composition that were computed using mBJ. Li-s states have a modest role in the development of the valence band, while Cu-4d, In-5p, and Cl/Br/I-p states play a substantial role. Cu-4d states have the largest density of states while Li-s states have the lowest. While the p-state of In and X went closer the band edge in the valence band, the greatest density states of Cu-4d traveled further into the valence band. The 3p/4p/5p states of halogens and the 5p states of In are crucial in the development of conduction band edges. When the size of the halogens in Li_2CuInX_6, these states dramatically shift closer the Fermi level and give improved information about bandgap decrease in the entire situation [33].

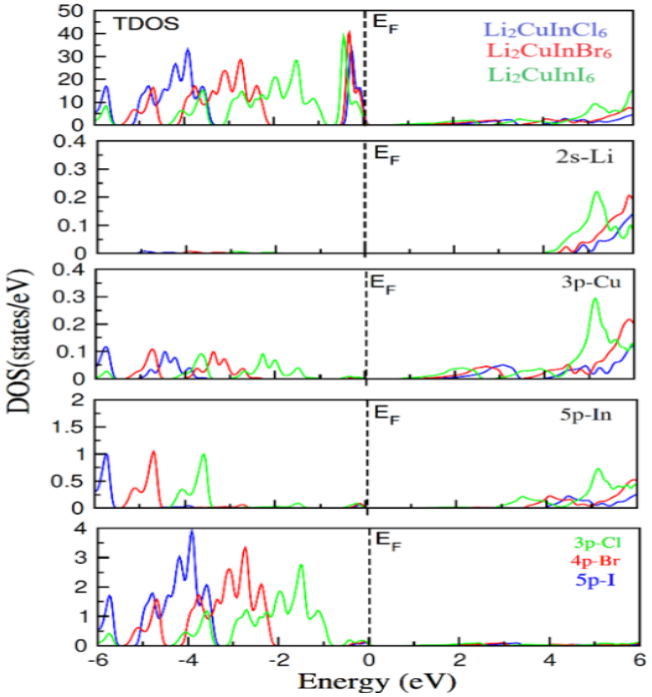

Fig. 4. Calculated total density of stated (DOS) along with partial DOS DPHs Li_2CuInX_6.

Materials optical characteristics are totally depend on connection between light and matter, therefore, optical behavior of materials are important to discuss within incident photon energy 0-14 eV. In optical characteristics, interaction assesses the likelihood of electron inter-band

transition and recombination rate as a result. The Kramer-Kronig formula was used to compute the optical response. The dielectric constants are used to analyze optical properties that depend on real $\varepsilon_1(\omega)$ and imaginary $\varepsilon_2(\omega)$ part. Similarly other optical parameters are obtained through dielectric constants. Fig. 5(a, b) illustrates the calculated $\varepsilon_1(\omega)$ and $\varepsilon_2(\omega)$ vs energy levels. The static value of the dielectric constant, often known as the $\varepsilon_1(0)$ value, is determined by the composition's polarization. Each compound's capacity to polarize relies on the polarizability of the constituent components, which in turn depends on the electronic cloud's size. For $Li_2CuInCl_6/Li_2CuInBr_6/Li_2CuInI_6$, the $\varepsilon_1(0)$ is estimated as 2.2/2.6/3.6, respectively. The energy value of $\varepsilon_1(\omega)$ rose along the rise of incoming light and produced peaks for $Li_2CuInCl_6$ at 6.2, 4.4, and 2.2 eV. When Cl replace with Br and I, these peaks migrated to lower energies. Additionally, for Li_2CuInI_6, the value of $\varepsilon_1(\omega)$ turned negative when the incoming radiation energy surpassed 8 eV to 14 eV, revealing its metallic nature in the high energy range [34]. Penn's model identified an inverse relationship between the bandgap energy and the $\varepsilon_1(0)$ dielectric constant, which is $\varepsilon_1(0) = 1+(\hbar\omega_p/E_g)^2$, where $\hbar$ stands for the minimized Planck's constant and ω_p is the plasma frequency.

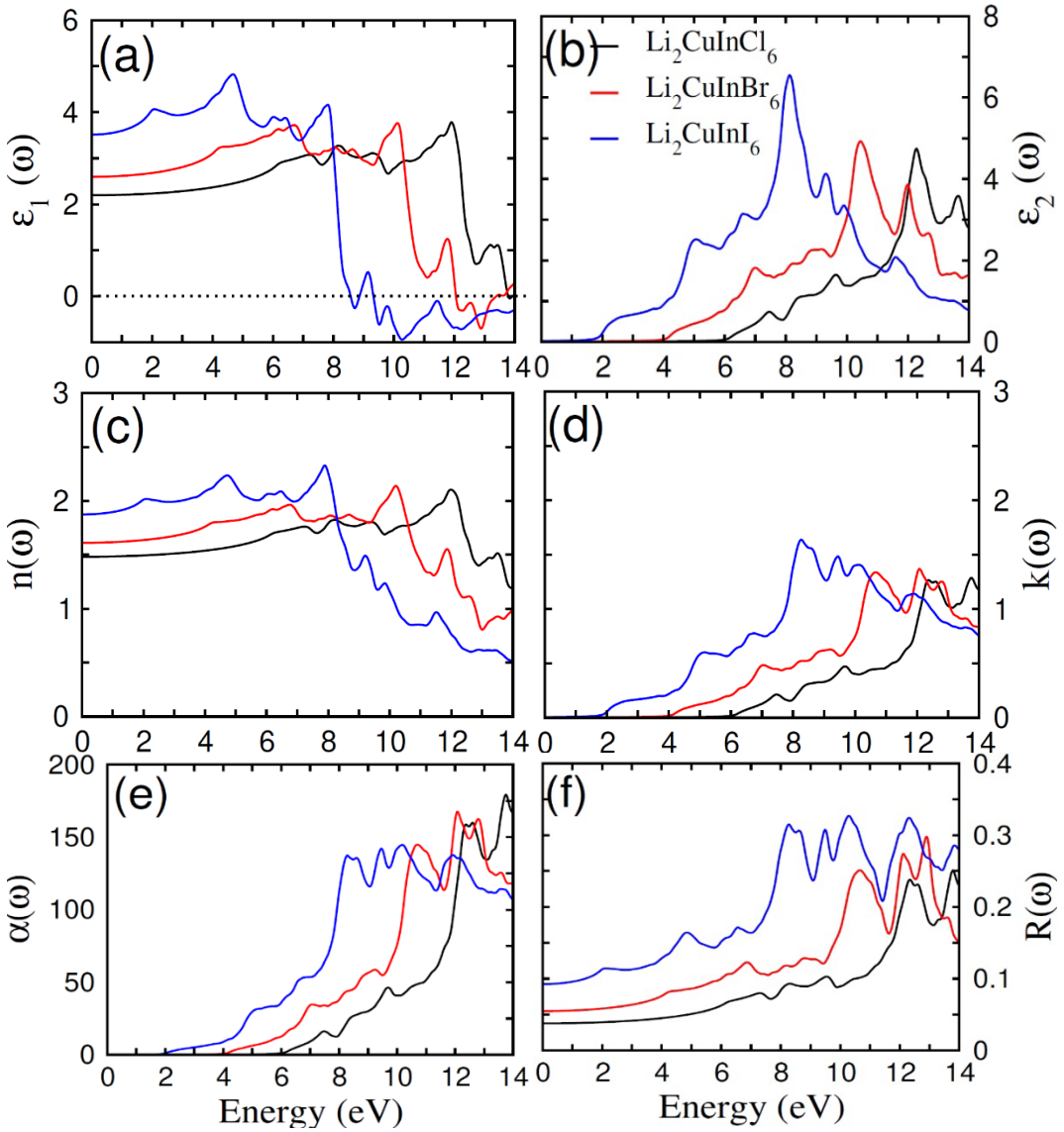

Fig. 5. Representation of (a) real part $\varepsilon_1(\omega)$, (b) imaginary part $\varepsilon_1(\omega)$, (c) refractive index $n(\omega)$, (d) the extinction co-efficient $k(\omega)$, (e) absorption $\alpha(\omega)$, (f) reflectivity $R(\omega)$ of DPHs Li_2CuInX_6.

When selecting opto-electronic materials for device construction, computing an imagined component $\varepsilon_2(\omega)$ is crucial. Therefore, it concentrates on the area of the electromagnetic range where materials are in touch and absorb more energy. Fig. 5(b) shows the reaction of $\varepsilon_2(\omega)$ to energy ranging from 0 to 14 eV. Below a specific level of incoming radiation energy, the value of $\varepsilon_2(\omega)$ is zero, and the threshold values of $\varepsilon_2(\omega)$ link to the absorption border, indicating the bandgap edge of the materials [35]. Numerous peaks in $\varepsilon_2(\omega)$ spectra indicate the presence of numerous resonators in each composition. At 7.4 eV, initial peak value for $Li_2CuInCl_6$ is appear, then replacing the halogen atoms Cl with Br and I, shift caused in lower energy. All compositions' refractive index versus energy spectra are displayed in Fig. 5(c), which offers important details on bandgaps, absorption behavior, and dispersion properties related to how light interacts with matter.

Refractive index and dielectric constant are related by the formula $n^2(0) = \varepsilon_1(0)$. This is thus because changes in $n(\omega)$ with energy are identical to changes in $\varepsilon_1(0)$. For optoelectronic gadgets, a refractive $n(\omega)$ index value in the range of 2 to 6 eV is suitable (see Fig. 5c). In Fig. 5(d), the extinction $k(\omega)$ co-efficient reacts similarly to incident photon energy as compared to $\varepsilon_2(\omega)$. In academic disciplines, such as optoelectronics, a recognition of a material's optical absorption is essential. It offers knowledge about the appropriateness of materials for certain uses, creates materials with required optical characteristics, and enhances the functionality of devices. A peak of $\varepsilon_2(\omega)$ and $k(\omega)$ signals the electron's shift from the valence-conduction state [36]. Fig. 5(e) shows the progression of the absorption (α) coefficient in relation to energy. For $Li_2CuInCl_6$, the value of rose from 1 eV and displayed several peaks. Distinct inter-band shifting possibilities are shown by the appearance of distinct peaks with different intensities. The reflectivity $R(\omega)$ values that are enhanced by chlorine, bromine, and iodine (see Fig. 5f). The increase in halogen atom size is responsible for this increase in reflectivity $R(\omega)$ value. In the IR and visible ranges, the value of $R(\omega)$ stays pretty steady, but in the UV region, it exhibits a large change.

3.3. Thermoelectric features

Although, it gives a numerical indicator of a material's capacity to convert heat energy into electrical energy and vice versa, calculating a material's thermoelectric efficiency (ZT) is crucial. An effective thermoelectric material has a higher value of ZT, which is expressed as $ZT = S^2\sigma T/\kappa$ [37]. Large voltage production and minimal electrical losses are provided by electrical conductivities and Seebeck coefficients that are high. Additionally, low thermal conductivity is necessary for modest heat losses. Electronic transition (k_e) and lattice vibration (k_ℓ) both contribute to thermal conductivity. BoltzTraP is used for computing the (k_e) value, however it is unable to determine the k_l value [38]. Additionally, relaxation time (10^{-14} s), which is the result of the system's atomic collision, divides electrical conductivity (σ) and lattice vibration k_ℓ. The performance of the compound's thermoelectricity is determined by its larger Seebeck coefficient, higher electrical conductivity, and lower thermal conductivity. The Fermi level lies between CB and VB, where electronic migration approaching CB from VB may occur, and giving rise to positively charged holes. A number of n-type materials are said to have electrons, however many p-type materials are said to contain holes [39]. The Seebeck coefficient, which is calculated by observing variation in voltage as a function of temperature, is written as beneath:

$$S = \frac{\mu \Delta V}{\Delta T} \tag{2}$$

Figure 6b shows the variance in the Seebeck coefficient as a function of temperature. At 300K, the S values for DPHs $Li_2CuInCl_6$, $Li_2CuInBr_6$ and Li_2CuInI_6 were 160, 178, and 188 μV/K, respectively. As the temperature increased, these values progressively declined. For the investigated DPs at 800 K, the S values were about 120 μV/K, 131 μV/K and 153 μV/K respectively. Thus the intensity of the induced voltage would be reduced as the temperature rose, more interactions would occur. Fig. 6a shows the electrical conductivity (σ/τ) figures that were calculated. The observed values of σ/τ are 0.6×10^{19} Ωms^{-1}, for all DPHs at 300 K. It was discovered that the electrical and thermal conductivities followed the same pattern. The Fronz-Wiedmann rule [40] states that the primary source of greater electrical conductivity is thermal vibrations. It's vital to note that k_e/τ in the investigated spinels did not include lattice thermal

conductivity. For the examined DPs, k_e/τ had an average of about 0.8×10^{14} (W/K^2ms) at room temperature, but stayed increases following a linear temperature rise up to 800K, leaving no discernible distinction among the two (see Fig. 6c).

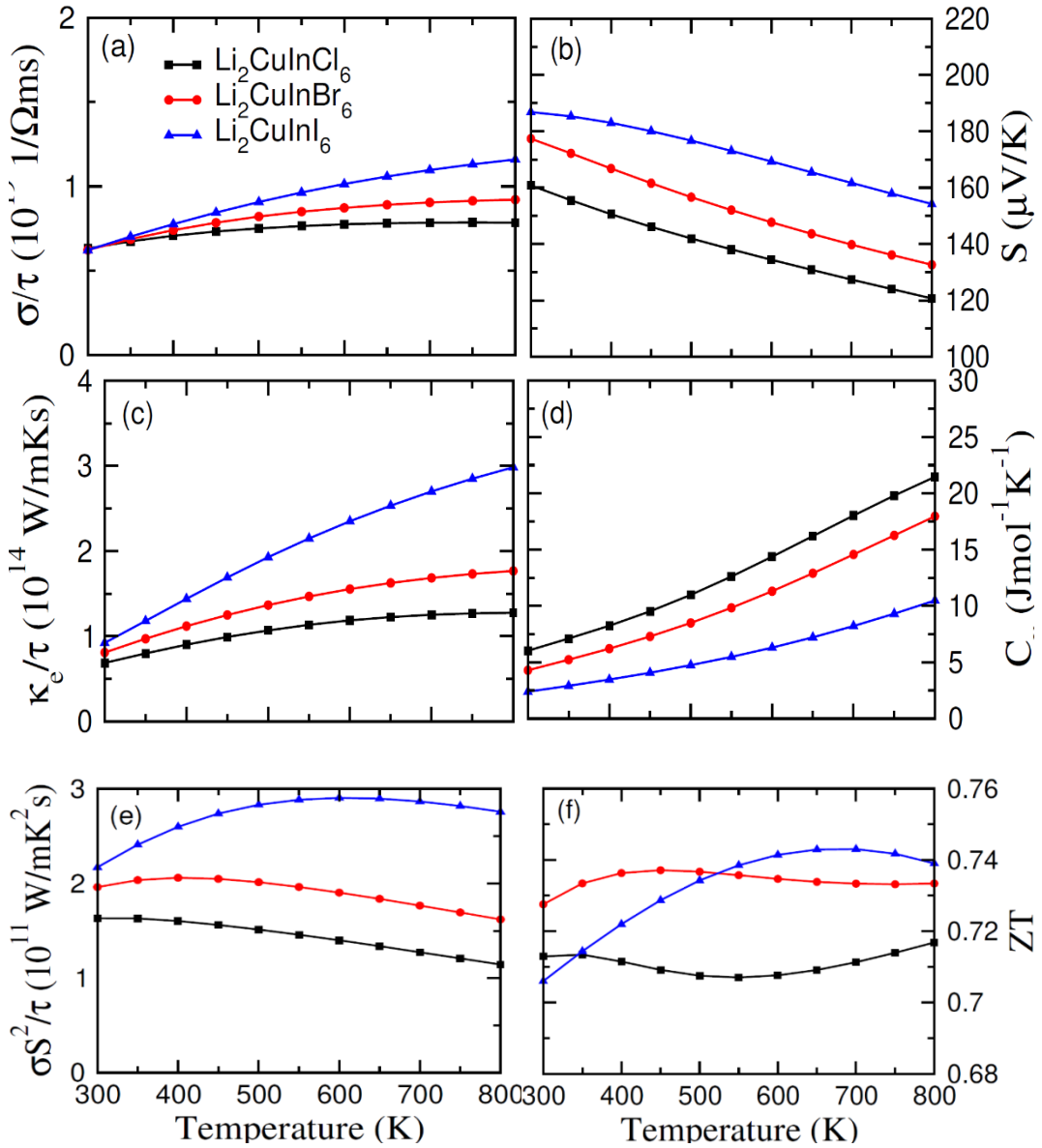

Fig. 6. The calculated (a) electrical conductivity (σ/τ), (b) Seebeck coefficients (S), (c) thermal conductivity (k_e/τ), (d) Specific heat capacity (Cv), (e) power factor and (f) figure of merit against temperature of DPHs Li_2CuInX_6.

The proportion of the specimen's total heat energy to the thermal variation that was created is how heat capacity (C_v) versus temperatures between 300 K and 800 K is calculated [41]. For the examined DPs, C_v also begins to rise with rising temperature (see Fig. 6d). For DPHs $Li_2CuInCl_6$, $Li_2CuInBr_6$ and Li_2CuInI_6, the values of C_v at room temperature are 6 J mol^{-1} K^{-1}, 4.5 J mol^{-1} K^{-1}, and 2.5 J mol^{-1} K^{-1}, correspondingly. Figure 6e displays the power factor ($s^2\sigma$) at temperatures between 300 K and 800 K. At 300 K, the power factor was $1.6\times10^{11}W/K^2ms$, $2.0\times10^{11}W/K^2ms$ and $2.2\times10^{11}W/K^2ms$ for DPHs $Li_2CuInCl_6$, $Li_2CuInBr_6$ and Li_2CuInI_6 when the temperature rose to 400 K, it continued to decreases. In Fig. 6f, the computed figure of merit (ZT) for temperature variations is shown. The value reported for Li_2CuInI_6 is 0.73 at 300K. This number has risen as a

result of additional temperature increases up to 500 K. Following then, it starts to decrease constantly even as the temperature rises to 800K. The similar pattern is also seen for $Li_2CuInCl_6$ and $Li_2CuInBr_6$, whose values were barely modified as the temperature increased.

4. Conclusion

In the present study, DFT was used to analyze the structural stability, optoelectronic, and thermoelectric performance of DPHs Li_2CuInX_6 (X= Cl, Br, I). The examined compounds' thermodynamic stability was validated by the computed formation of production. The DP $Li_2CuInCl_6$ with the greatest value of -2.43 eV, was the most stable. Their ductile nature was verified by the computed Poisson's (>0.26) and Pugh's ratio (>1.75) values. The definition of the borders of electronic bands was greatly aided by the hybridization of the d-states of Cu and halogens as well as In atoms p-state. Direct bandgaps values of 1.34 eV for Cl, 0.84 eV for Br, and 0.34 eV from band structure plot indicating potential applications in optoelectronic devices. Further, maximum absorption appear in visible and IR region justified that all DPHs are potentially used in optoelectronic devices. Additionally, extremely low thermal conductivity scales, better Seebeck coefficient significantly increased the figure of merit (ZT). The examined materials stand out for their greater ZT at room temperature values and absorption in the visible region, which make them appropriate for renewable energy systems. As a result, experimental researchers could identify these chemicals for photovoltaic cells and thermoelectric appliances.

Funding information

Researchers Supporting Project number (RSP2024R118), King Saud University.

Acknowledgements

The authors would like to thank Researchers Supporting Project number (RSP2024R118), King Saud University, Riyadh, Saudi Arabia

References

[1] Bhamu, K. C., Soni, A., Sahariya, J. (2018), Solar Energy, 162, 336-343; https://doi.org/10.1016/j.solener.2018.01.059

[2] Shah, S. Z. A., Niaz, S. (2021), Materials Today Communications, 28, 102609; https://doi.org/10.1016/j.mtcomm.2021.102609

[3] Qazi, A., Hussain, F., Rahim, N. A., Hardaker, G., Alghazzawi, D., Shaban, K., Haruna, K. (2019), IEEE access, 7, 63837-63851; https://doi.org/10.1109/ACCESS.2019.2906402

[4] Sharma, P. K., Senguttuvan, T. D., Sharma, V. K., Chaudhary, S. (2021), Materials Today Energy, 21, 100713; https://doi.org/10.1016/j.mtener.2021.100713

[5] Elavarasan, R. M., Leoponraj, S., Vishnupriyan, J., Dheeraj, A., Sundar, G. G. (2021), Renewable Energy, 170, 1396-1426; https://doi.org/10.1016/j.renene.2021.01.134

[6] Østergaard, P. A., Duic, N., Noorollahi, Y., Mikulcic, H., Kalogirou, S. (2020), Renewable Energy, 146, 2430-2437; https://doi.org/10.1016/j.renene.2019.08.094

[7] Sun, J., Singh, D. J. (2016), APL Materials, 4(10), 104803; https://doi.org/10.1063/1.4952610

[8] Saxena, M., Balani, K., Maiti, T., (2019), Materials Science and Engineering: B, 244, 65-71; https://doi.org/10.1016/j.mseb.2019.04.025

[9] Usman, M., Yan, Q. (2020), Crystals, 10(2), 62; https://doi.org/10.3390/cryst10020062

[10] Divitini, G., Cacovich, S., Matteocci, F., Cinà, L., Di Carlo, A., Ducati, C. (2016), Nature Energy, 1(2), 1-6; https://doi.org/10.1038/nenergy.2015.12

[11] Zhao, X. G., Yang, J. H., Fu, Y., Yang, D., Xu, Q., Yu, L., Zhang, L. (2017), Journal of the American Chemical Society, 139(7), 2630-2638; https://doi.org/10.1021/jacs.6b09645

[12] Rogl, G., Rogl, P. (2017), Current opinion in green and sustainable chemistry, 4, 50-57; https://doi.org/10.1016/j.cogsc.2017.02.006

[13] Ali, M. A., Dar, S. A., AlObaid, A. A., Al-Muhimeed, T. I., Hegazy, H. H., Nazir, G., Murtaza, G. (2021), Journal of Physics and Chemistry of Solids, 159, 110258; https://doi.org/10.1016/j.jpcs.2021.110258

[14] Haq, A. U., Mustafa, G. M., Amin, M., Ramay, S. M., Mahmood, A. (2021), International Journal of Energy Research, 45(6), 9241-9251; https://doi.org/10.1002/er.6455

[15] Nabi, M., Bhat, T. M., & Gupta, D. C. (2019), International Journal of Energy Research, 43(9), 4229-4242; https://doi.org/10.1002/er.4547

[16] Madsen, G. K., Singh, D. J. (2006), Computer Physics Communications, 175(1), 67-71; https://doi.org/10.1016/j.cpc.2006.03.007

[17] Blaha, P., Schwarz, K., Tran, F., Laskowski, R., Madsen, G. K., Marks, L. D. (2020), The Journal of chemical physics, 152(7), 074101; https://doi.org/10.1063/1.5143061

[18] Elhag, A. (2018), Results in Physics, 9, 793-805; https://doi.org/10.1016/j.rinp.2018.03.055

[19] Madsen, G. K., Carrete, J., Verstraete, M. J. (2018), Computer Physics Communications, 231, 140-145; https://doi.org/10.1016/j.cpc.2018.05.010

[20] Fedorovskiy, A. E., Drigo, N. A., Nazeeruddin, M. K. (2020), Small Methods, 4(5), 1900426; https://doi.org/10.1002/smtd.201900426

[21] Mahmood, Q., Ghrib, T., Rached, A., Laref, A., Kamran, M. A. (2020), Materials Science in Semiconductor Processing, 112, 105009; https://doi.org/10.1016/j.mssp.2020.105009

[22] Bartel, C. J., Sutton, C., Goldsmith, B. R., Ouyang, R., Musgrave, C. B., Ghiringhelli, L. M., Scheffler, M. (2019), Science advances, 5(2), eaav0693; https://doi.org/10.1126/sciadv.aav0693

[23] Young, J., Rondinelli, J. M. (2016), The journal of physical chemistry letters, 7(5), 918-922; https://doi.org/10.1021/acs.jpclett.6b00094

[24] Ahn, C. W., Jo, J. H., Kim, J. C., Ullah, H., Ryu, S., Hwang, Y., Kim, T. H. (2020); Journal of Materiomics, 6(4), 651-660; https://doi.org/10.1016/j.jmat.2020.05.008

[25] Jong, U. G., Yu, C. J., Kye, Y. H., Choe, S. H., Kim, J. S., Choe, Y. G. (2019), Physical Review B, 99(18), 184105; https://doi.org/10.1103/PhysRevB.99.184105

[26] Jong, U. G., Yu, C. J., Kye, Y. H. (2020), RSC advances, 10(1), 201-209; https://doi.org/10.1039/C9RA09232C

[27] Roknuzzaman, M., Ostrikov, K., Wang, H., Du, A., Tesfamichael, T. (2017), Scientific reports, 7(1), 14025; https://doi.org/10.1038/s41598-017-13172-y

[28] Noor, N. A., Mahmood, Q., Rashid, M., Haq, B. U., Laref, A. (2018), Ceramics International, 44(12), 13750-13756; https://doi.org/10.1016/j.ceramint.2018.04.217

[29] Bobrov, V. B., Trigger, S. A., Van Heijst, G. J. F., Schram, P. P. J. M. (2010), Europhysics Letters, 90(1), 10003; https://doi.org/10.1209/0295-5075/90/10003

[30] Ciftci, Y. O., Colakoglu, K., Deligoz, E., Ozisik, H. (2008), Materials Chemistry and Physics, 108(1), 120-123; https://doi.org/10.1016/j.matchemphys.2007.09.012

[31] Wang, N., Zhou, Y., Ju, M. G., Garces, H. F., Ding, T., Pang, S., Sun, X. W. (2016), Advanced Energy Materials, 6(24), 1601130; https://doi.org/10.1002/aenm.201601130

[32] Zhou, L., Liao, J. F., Huang, Z. G., Wang, X. D., Xu, Y. F., Chen, H. Y., Su, C. Y. (2018), ACS Energy Letters, 3(10), 2613-2619; https://doi.org/10.1021/acsenergylett.8b01770

[33] Saliba, M., Matsui, T., Domanski, K., Seo, J. Y., Ummadisingu, A., Zakeeruddin, S. M., Grätzel, M. (2016), Science, 354(6309), 206-209; https://doi.org/10.1126/science.aah5557

[34] Haq, B. U., AlFaify, S., Ahmed, R., Butt, F. K., Laref, A., Shkir, M. (2018), Physical Review B, 97(7), 075438; https://doi.org/10.1103/PhysRevB.97.075438

[35] Marathe, M., Grünebohm, A., Nishimatsu, T., Entel, P., Ederer, C. (2016), Physical Review

B, 93(5), 054110; https://doi.org/10.1103/PhysRevB.93.054110

[36] Saeed, Y., Amin, B., Khalil, H., Rehman, F., Ali, H., Khan, M. I., Shafiq, M. (2020), RSC advances; https://doi.org/10.1039/D0RA90062A

[37] Dolling, G., Enkrich, C., Wegener, M., Soukoulis, C. M., Linden, S. (2006), Science, 312(5775), 892-894; https://doi.org/10.1126/science.1126021

[38] Arribi, P. V., García-Fernández, P., Junquera, J., Pardo, V. (2016), Physical Review B, 94(3), 035124; https://doi.org/10.1103/PhysRevB.94.035124

[39] Wu, T., Gao, P. (2018), Materials, 11(6), 999; https://doi.org/10.3390/ma11060999

[40] Li, J., Ma, Z., Sa, R., & Wu, K. (2017), RSC advances, 7(52), 32703-32709; https://doi.org/10.1039/C7RA05193J

[41] Khan, T. T., Ur, S. C. (2018), Electronic Materials Letters, 14, 336-341; https://doi.org/10.1007/s13391-018-0029-y